

Molecular Simulation

ISSN: (Print) (Online) Journal homepage: https://www.tandfonline.com/loi/gmos20

Insight into the structural, thermal and ion transport properties of solid and liquid Mg_3N_2: a model potential and NPT molecular dynamics simulation

Yenal Aydın, Seçkin D. Günay, Ünsal Akdere & Çetin Taşseven

To cite this article: Yenal Aydın, Seçkin D. Günay, Ünsal Akdere & Çetin Taşseven (2022) Insight into the structural, thermal and ion transport properties of solid and liquid Mg_3N_2: a model potential and NPT molecular dynamics simulation, Molecular Simulation, 48:7, 602-609, DOI: 10.1080/08927022.2022.2039389

To link to this article: https://doi.org/10.1080/08927022.2022.2039389

Published online: 18 Feb 2022.

Submit your article to this journal

Article views: 80

View related articles

View Crossmark data

Full Terms & Conditions of access and use can be found at
https://www.tandfonline.com/action/journalInformation?journalCode=gmos20

MOLECULAR SIMULATION
2022, VOL. 48, NO. 7, 602–609
https://doi.org/10.1080/08927022.2022.2039389

Taylor & Francis
Taylor & Francis Group

Check for updates

Insight into the structural, thermal and ion transport properties of solid and liquid Mg_3N_2: a model potential and NPT molecular dynamics simulation

Yenal Aydın, Seçkin D. Günay, Ünsal Akdere and Çetin Taşseven

Department of Physics, Yıldız Technical University, İstanbul, Turkey

ABSTRACT

A model potential has been developed for magnesium nitride (Mg_3N_2) by fitting the parameters to an experimental lattice constant and bulk modulus. The mechanical properties have been calculated at 0 K. The potential was tested by molecular dynamics simulation at constant number, volume and energy ensemble at 300 K. The structural, ion transport and thermodynamic properties were investigated at a constant number and pressure–temperature ensemble between 300 and 2500 K. The simulated XRD diffractogram at 300 K shows that the crystalline peaks with corresponding (hkl) planes are correctly reproduced. A solid–liquid transition occurs at about 1800 K with a marked variation in all calculated physical properties. The potential successfully models the interactions in Mg_3N_2 at the solid and liquid phases. The results presented in this paper fill the gap of theoretical study in literature and extend our knowledge further, which could be useful to pave the way for the search of functional materials.

ARTICLE HISTORY
Received 7 October 2021
Accepted 2 February 2022

KEYWORDS
Magnesium nitride; model potential; physicochemical properties; molecular dynamics simulation

1. Introduction

Magnesium nitride (Mg_3N_2) is a II-V group semiconductor with various technological and industrial applications owing to its salient physicochemical properties. Mg_3N_2 is generally used to prepare metal and non-metal nitrides [1–4] and as a catalyst to synthesise superhard cubic boron nitrides and silicon nitride ceramics [1,5]. Over the last decade, Mg_3N_2 powder has received growing attention as it formed hydrogen storage material owing to the reversible reaction between Mg_3N_2 and H_2 forming $Mg(NH_2)_2$ and MgH_2 [6–8]. Moreover, it is also used as an optoelectronic light-emitting semiconducting material [9] and as an additive in the refinement process of steel [10]. Molten magnesium antimonide (Mg_3Sb_2) has also been used as an electrolyte in the energy storage system called the ambipolar electrolysis cell [11]. This contains the liquid state of magnesium and antimony as the top and the bottom electrode layers, and molten salt as the ionically conductive electrolyte in the middle layer, all of which are immiscible liquids operating at about 1000 K. On account of the search of potential functional materials for electronic and optoelectronic applications, the structural, electronic, optical and thermoelectric properties of magnesium pnictides Mg_3X_2(X = N, P, As, Sb, Bi) [12] and alkaline-earth nitrides M_3N_2(M = Mg, Be, Ca) [13] have been examined by the density functional theory (DFT) calculation. Previously, our group has reported the structural, ionic transport and thermophysical properties of the solid and liquid forms of three members of magnesium pnictides (Mg_3Bi_2 [14], Mg_3Sb_2 [15] and Mg_3As_2 [16]) using the hypernetted-chain theory of liquids (HNC) and the molecular dynamics simulation (MD) in conjunction with a semi-empirical pairwise potential.

Notwithstanding its technological and industrial importance, the fundamental properties of Mg_3N_2 are barely studied in the literature. To fill this gap, we would like to systematically investigate the structural, thermal and ionic transport properties within a wide range of temperatures at the solid and liquid phases by means of the classical computer simulation method at constant pressure. The present work will be beneficial to adjust the thermophysical properties in searching functional materials in the area of applications Mg_3N_2 based on solid and liquid forms. Furthermore, the results extend our knowledge on the structural, thermal and ionic diffusion, and provide a newly developed pairwise potential for future theoretical studies.

2. Procedure

X-ray structure analysis has confirmed that crystal magnesium nitride, Mg_3N_2, has the cubic antibixbyite structure with the space group of Ia3 (&*num*; 206) and lattice parameter $a = 997.26$pm [17]. The classical molecular dynamics simulation describes the motion of particles using the force calculated by the numerical integration of Newton's equation of motion for a large number of particles. It relies on a mathematical definition of the interatomic interactions that is generally an analytical function.

2.1. Potential

The interaction between ionic species Mg^{2+} and N^{3-} has been modelled with the Buckingham type of rigid-ion pairwise

CONTACT Çetin Taşseven tasseven@yildiz.edu.tr
© 2022 Informa UK Limited, trading as Taylor & Francis Group

potential of the form [18]

$$\phi_{ij}(r) = \frac{Z_i Z_j e^2}{r} + A_{ij}\exp\left(-\frac{r}{\rho_{ij}}\right) - \frac{C_{ij}}{r^6} \quad (1)$$

The first, second and third terms, respectively, represent the Coulomb interactions with the effective charges of $Z_{i,j}$, the short-range repulsive interactions due to the Pauli exclusion principle and the van der Walls attractive interactions. The parameters of strength $A_{i,j}$, hardness $\rho_{i,j}$ and van der Walls $C_{i,j}$, and the effective charges $Z_{i,j}$ were obtained by the trial-error method by fitting to experimental and first-principles lattice constant and bulk modulus, using the general utility lattice program (GULP) [19]. In addition, the phase transition temperature (solid→liquid) during NPT simulation was also taken into account in determining the parameters. The estimated values for the parameters of the potential are listed in Table 1.

2.2. Mechanical properties

Following the fitting process, the lattice constant and bulk optimization run is performed. The lattice constant and the mechanical properties were calculated and are presented in Table 2 together with the DFT and experimental data available in the literature [20–25]. There are only three independent elastic constants for the cubic antibixbyite single crystal (C_{11}, C_{12} and C_{44}).

The Voigt-Reuss-Hill approximation is used to calculate the mechanical properties [26–28]: bulk modulus (K), shear modulus (G_V, G_R, G_H), Young's modulus (E), Poisson's ratio (υ) and the Zener anisotropy factor A. The high value of $C_{11} - C_{12}$ and Young's modulus indicate the poor plasticity of Mg_3N_2. While the poor plasticity is also supported by Poisson's ratio, the ductility condition $C_{12} - C_{44} > 0$ is satisfied. The ratio of the shear modulus to bulk modulus (G_H/K) is very close to the ductility/brittleness critical value of 0.5 [29,30]. The Zener anisotropy ratio A defines the degree of elastic anisotropy in cubic crystals, which approaches the unity of 1 for isotropic materials [31]. The Zener factor of Mg_3N_2 deviates about 12% from the unity. We must note that inaccurate prediction of some mechanical properties, especially, elastic constants (C_{11} and C_{12}) and ductile behavior of the material, which is supposed to be brittle according to DFT calculations [22], does not affect the validity of our work whose desire is to investigate the thermal evolution of the structure, thermodynamic and ion transport properties from the solid to liquid phase with a model potential of a single set of parameters.

2.3. Molecular dynamics simulation

The MD simulation was performed with MOLDY code [32] using the microcanonical NVE (constant number, volume and energy) and the isobaric-isothermal NPT (constant number, pressure, and temperature) ensembles. Both the NVE and NPT simulation cells were constructed by setting the number of Mg^{+2} and N^{-3} ions as 3072 and 2048, respectively, in a box of 4 × 4 x 4. Ewald's sum method was used to handle the long-range Coulomb interactions with a 20 Å cutoff. The periodic boundary conditions were applied on the simulation cell to avoid the surface effects. The MD simulations include 100 ps run with time steps of $\Delta t = 0.005$ps. The first 30 ps is to reach the desired equilibrium state; then, the physical properties were calculated by averaging over the following 70 ps. Figure 1 represents the fluctuations in the desired temperature and total energy as a function of the MD step in the NVE ensemble at 300 K. Our average temperature remains constant during the course of simulation with a value of 300.04 ± 0.05. The average total energy per unit cell is −59622.34 ± 0.06 kJ/mole at 300K the NVE simulation.

First, we test our potential by the energy minimization criterion $\left(\frac{dE}{d\rho}\right)_T = 0$ in the NVE simulation at 300K. The cell parameter varied from 9.0 Å to 11.0 Å with 0.2 Å increments with the same simulation conditions summarised above. Figure 2 shows this minimization procedure as the internal energy per unit cell versus lattice parameter and density. The optimised cell parameter and density were, respectively, estimated as 9.89 Å and 2.774 g/ml which aggrege well with the literature value of 9.95 − 10.09 Å [21–25] and 2.712 g/ml [33]. The corresponding ground state energy is −59625, 53 kJ/mol per unit cell.

3. Results and discussions

Constant pressure-temperature (NPT) simulation was conducted by applying the Nosé-Hoover thermostat and Parrinello–Rahman constant stress method to control temperature and pressure. Once the system reached an equilibrium of which simulations were run for 30 ps, the properties of interests were calculated by averaging over the following 70 ps for the temperatures in the range of 300 to 2500 K at 50 K intervals.

X-ray powder diffraction pattern of Mg_3N_2 is simulated from the structure parameters calculated at 300 K in the NPT ensemble using the structural analysis program VESTA [34] and presented in Figure 3. The lattice planes were also

Table 1. Values for the potential parameters as the strength $A_{i,j}$, hardness $\rho_{i,j}$, van der Walls $C_{i,j}$. The effective charges are $Z_{Mg} = +1.135$ and $Z_N = -1.7025$.

Ion pair	$A_{i,j}(eV)$	$\rho_{i,j}$(Å)	$C_{i,j}$ (eVÅ^6)
Mg-Mg	2.37×10^6	0.152	0
Mg-N	3.57×10^3	0.247	35.53
N-N	11.41	0.868	10^{-6}

Table 2. The lattice constant and the mechanical properties of Mg_3N_2 in units of GPa at $T = 0K$ calculated using the general utility lattice program (GULP) [19].

Properties	This work	Experiment/First principal
a_0 (Å)	9.898	9.972 [20], 9.957 [21], 10.09 [22], 9.9528 [23], 9.955 [24]
K	110.8	109.3 [20], 104.6 [22], 104.8 [25]
G_V	58.63	73.5 [22], 71.5 [25]
G_R	58.46	
G_H	58.54	
E	149.33	178.7 [22], 174.7 [25]
C_{11}	183.82	237.3 [22]
C_{12}	74.30	25.3 [22]
C_{44}	61.21	59.5 [22]
υ	0.29	0.22 [22]
A	1.12	1.12 [22]
G_H/K	0.53	0.70 [22], 0.68 [25]

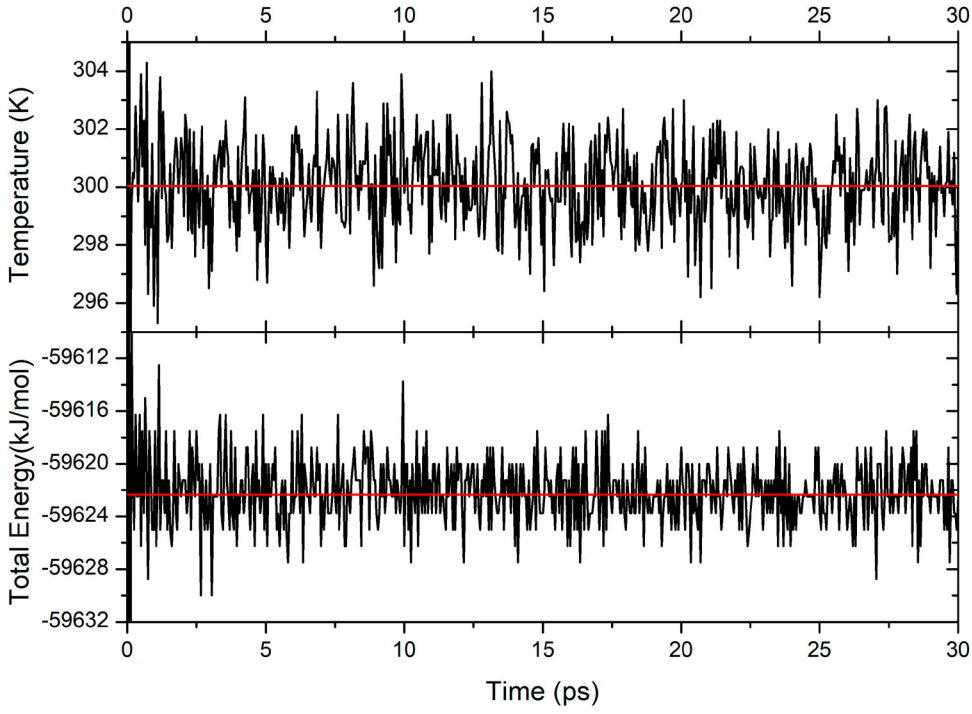


Figure 1. (Colour online) The evolution of temperature and total energy with time step.

calculated from Bragg's law and expressed as the Miller indices (hkl) for each crystalline peak in Figure 3. The simulated XRD diffractogram peaks with corresponding Bragg angle match correctly with the XRD patterns of the combustion synthesised Mg_3N_2 powders [35].

The radial distribution function (RDF) *gij*(*r*) gives the quantitative measurements of radial order of ions, one another. The running coordination number (RCN) *nij*(*r*) which is calculated by the integration of *gij*(*r*) in spherical coordinates is the number of ions in the range of each ion species. Figure 4 shows the radial distribution functions (solid lines) and the coordination numbers (dashed lines) of ionic pairs for representative five different temperatures of 300, 800, 1300, 1750 and 1800 K. The average nearest neighbor separation of ionic pairs is determined by the

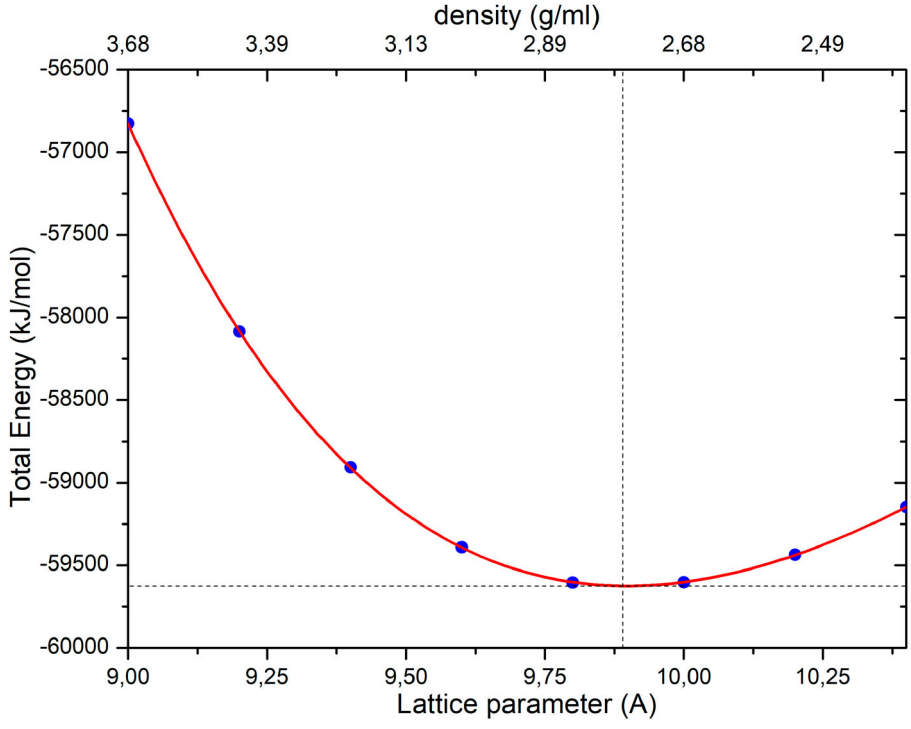


Figure 2. (Colour online) Unit cell energy of Mg_3N_2 versus volume and density at 300 K in the microcanonical NVE ensemble.

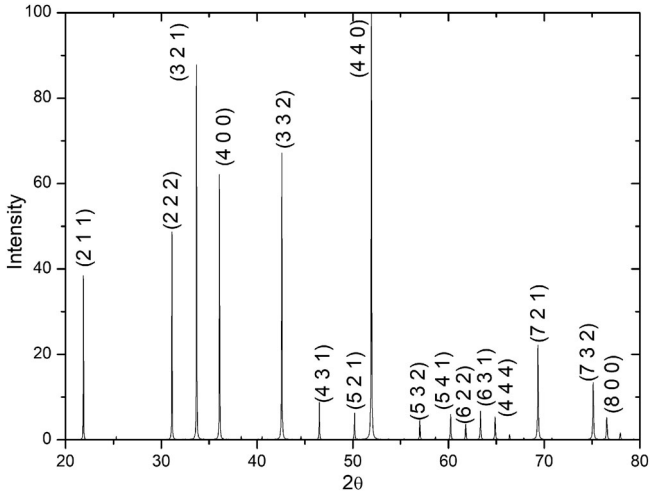


Figure 3. (Colour online) Simulated XRD pattern of magnesium nitride as intensity versus Bragg angle 2θ (degree).

position of the principal peak of $g_{ij}(r)$. The contact distance and the first coordination numbers at 300 K are estimated as $r_{MgN}^{\max} = 2.15\text{Å}$, $r_{MgMg}^{\max} = 2.75\text{Å}$ and $r_{NN}^{\max} = 3.35\text{Å}$, and $n_{MgN} = 4$, $n_{MgMg} = 6$ and $n_{NN} = 6$, respectively. The separations obtained in this work fall within the shortest distance range suggested by the first principal, $r_{MgN} = 2.11 - 2.21\text{Å}$, $r_{MgMg} = 2.75 - 2.99\text{Å}$ and $r_{NN} = 3.37 - 3.81\text{Å}$ [22], and experimental, $r_{MgN} = 2.08 - 2.18\text{Å}$, $r_{MgMg} = 2.72 - 2.95\text{Å}$ and $r_{NN} = 3.31 - 3.75\text{Å}$ [23], studies. The cumulative N-N coordination number of 12 calculated from the first two peaks of $g_{NN}(r)$ at 3.35Å and at 3.75Å agrees with the crystallographic data of 12 shortest N-N distances of Mg_3N_2 [23]. These two peaks gradually dissolve into a single peak as the temperature increases and become a broad single peak with $n_{NN} \cong 8$ at 1800K. Similar behavior is also observed for the Mg-Mg coordination. The $g_{MgN}(r)$ successfully reproduces that the Mg atoms have fourfold tetrahedral coordination neighboring N atoms at the solid phase which reduces to about 3 through melting. As shown in the inset in Figure 4, the separations of N-N and Mg-Mg pairs gradually increase between the temperatures of 300–1750 K, and exhibit a marked jump from 1750 to 1800 K. Contrarily, the nearest neighbor distance of Mg-N decreases up to 1750; then, it has a sudden drop. After 1800 K, all nearest neighbor separations remain constant, and $g_{ij}(r)$ of the anion and cation pairs display the characteristic features of an ionic melt. In addition, evidently, the stepwise behavior of RNC reflects the solid like behavior of the particles between 300 and 1750 K, while relatively continuous feature of the RNC at 1800 K indicate the liquid state. The coordination numbers for all three ionic pair are constant up to 1800 K. The present structural analysis of magnesium nitride with the NPT simulation signals that the solid–liquid transition occurs at about 1800 K which needs further justification with transport and thermal properties which is following.

The mean-square displacement (MSD) $r_i^2(t)$ is a useful tool to understand the diffusion process of ionic species and observe whether the system is in a solid or liquid phase. Moreover, the MSD allows you to estimate the self-diffusion coefficient D_i which plays an important role in many applications such as electrochemical devices. D_i is calculated by the geometrical slope at the linear regime of MSD using the well-known Einstein relation. The MSDs of magnesium and nitride ions are illustrated at eight temperatures in Figure 5 as a representative sample of all calculations. Almost zero asymptotic slopes of MSDs of both species up to about 1750K mean that both sublattices are at the solid state. Beyond 1750 K, the linear change of MSD is evident and indicates the liquid-like behavior of both ionic components. This is near the experimental melting temperature of 1500°C of powder Mg_3N_2 [33]. The snapshots of the simulation box at 300, 1750 and 1800 K shown as an inset in Figure 5 exhibit the visualization of the transition from the solid to liquid phase.

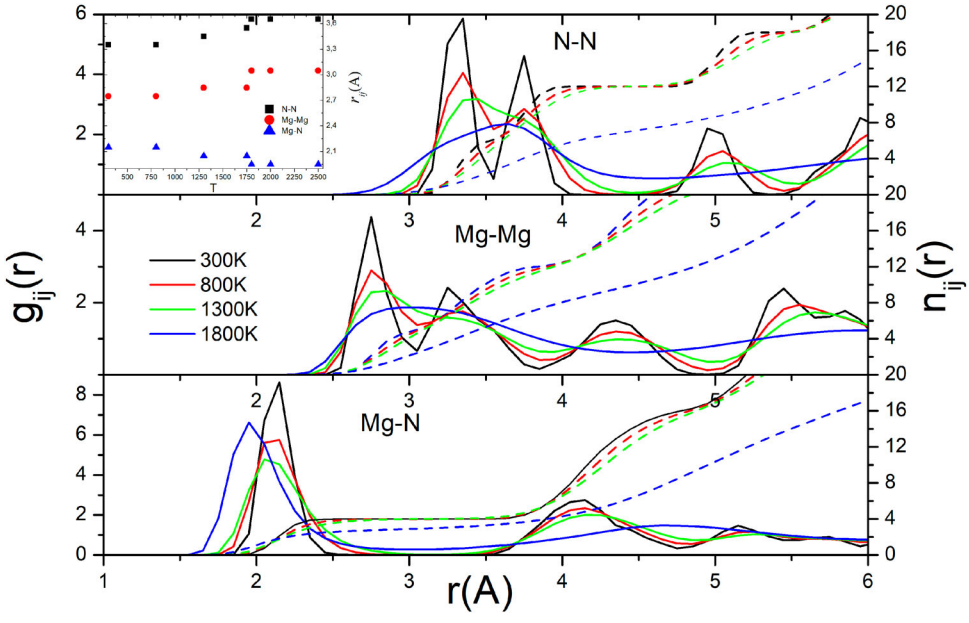


Figure 4. (Colour online) The radial distribution functions (solid lines) $g_{ij}(r)$ and the running coordination numbers (dashed lines) $n_{ij}(r)$ of ionic pairs for five different temperatures. The inset is the nearest neighbor separations versus temperature.

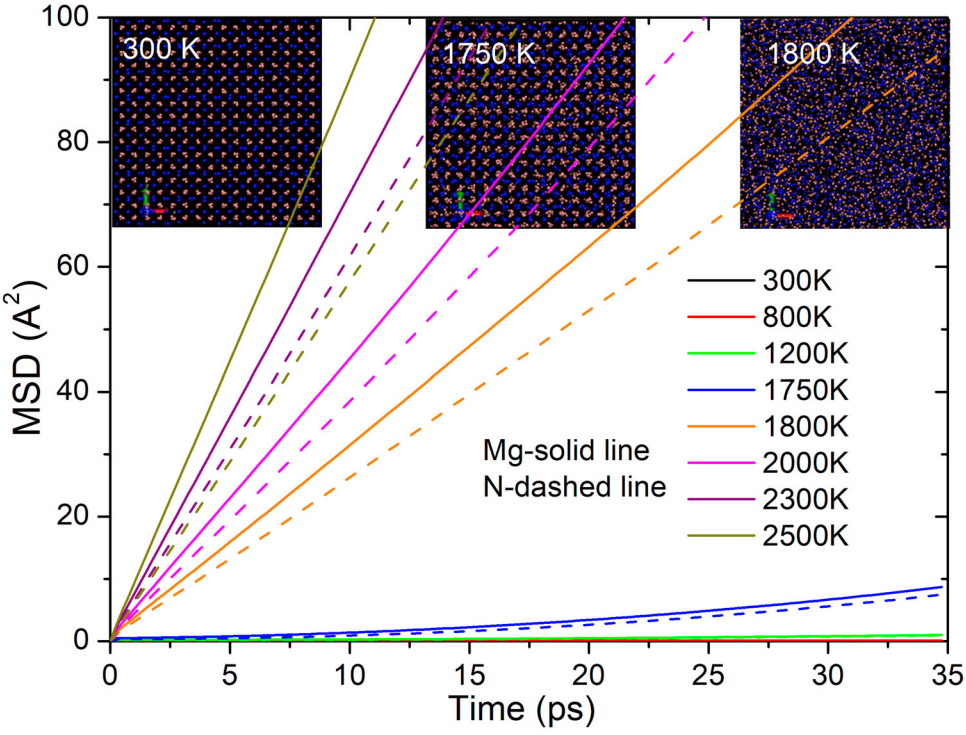


Figure 5. (Colour online) The mean square displacements of magnesium (solid lines) and nitride (dashed lines) ions. The insets are the snapshots of the simulation box at 300, 1750 and 1800 K.

The self-diffusion coefficients D_{Mg} and D_N were computed by Einstein's diffusion equation $D = \lim_{t\to\infty} \frac{1}{6t}\frac{1}{N}\sum_{i=1}^{N}[\vec{r}_i(t) - \vec{r}_i(0)]^2$ and are presented in Figure 6(a). The diffusion coefficient of both ions is zero up to about 800 K; then exhibits thermally agitated, very small mobility reaching the value of $\approx 10^{-6}$ cm^{2}s^{-1} at 1750 K. Upon melting, there is an abrupt jump to the value of $\approx 5\text{x}10^{-5}$ cm^{2}s^{-1} at 1800 K corresponding to a sudden increase in the diffusion of the ions in the liquid phase. The

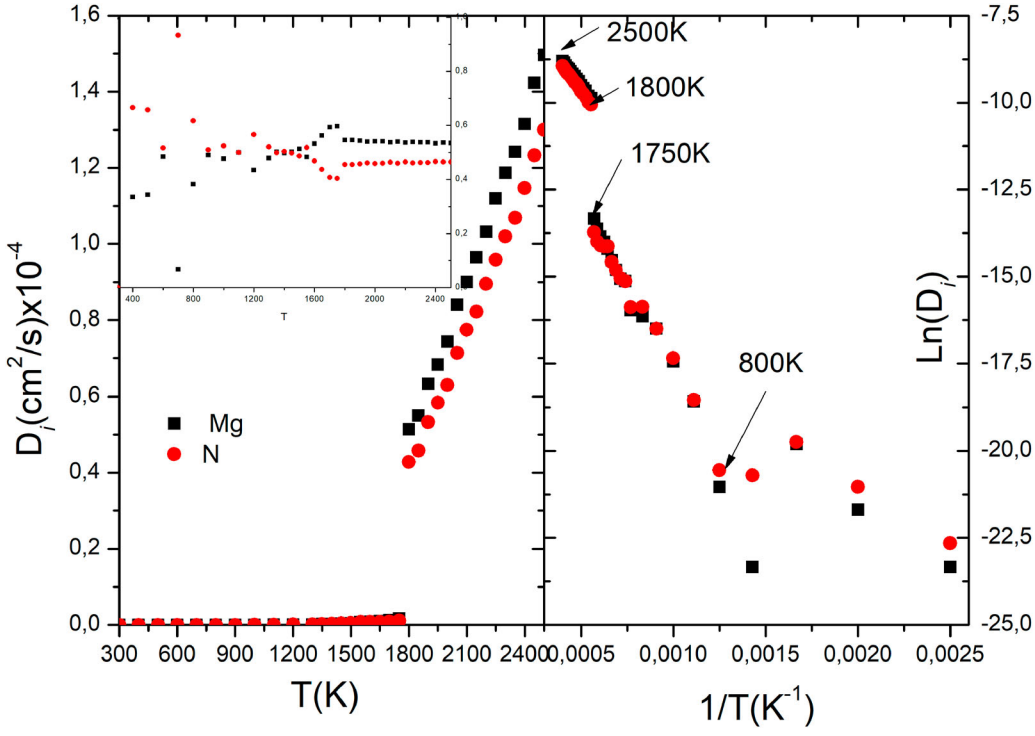


Figure 6. (Colour online) (a) The Einstein self-diffusion coefficients of magnesium and nitride ions, and (b) the Arrhenius plot of diffusion coefficients. The inset is the transference numbers versus temperature.

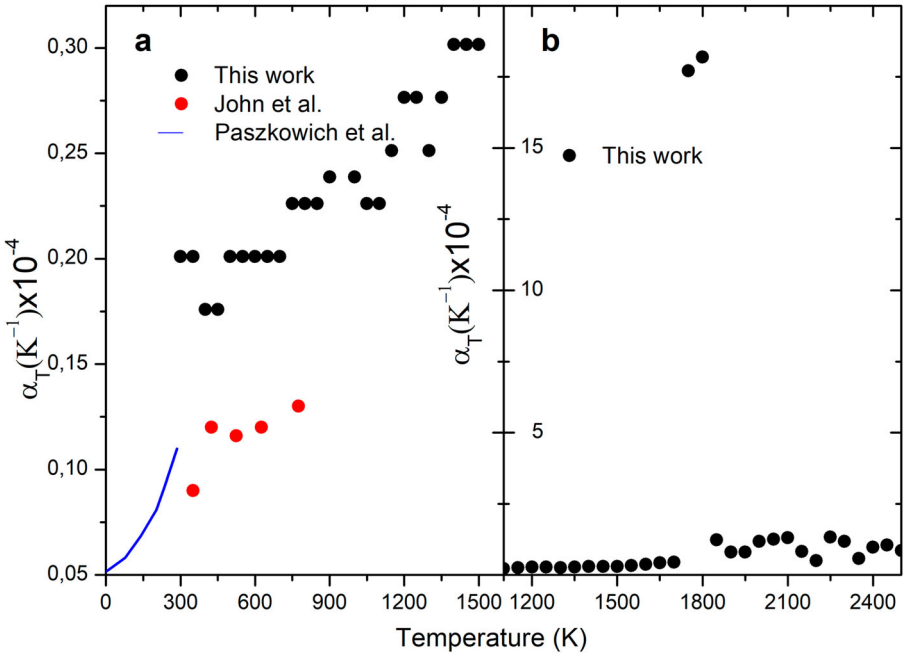


Figure 7. (Colour online) The linear thermal expansion coefficient (LTEC) (a) between $0K - 1500K$ and (b) between $1200K - 2500K$.

inset in Figure 6 a is the transference number which is defined as $t_i = \frac{D_i}{D_i + D_j}$ within the Nernst–Einstein framework. As both ions exhibit almost zero diffusion up to about 800K, the scattered data before this temperature have no physical significance and is due to uncertainties in calculations. The mass and size ratios between nitrogen and magnesium ions, respectively, are $\frac{M_N}{M_{Mg}} \cong 0.6$ and $\frac{r_N}{r_{Mg}} \cong 2.5$. Evidently, from 800K to about 1300K, nitrogen ions are slightly more diffusive than magnesium as a result of being the lighter atom. Up to about 1600K, the diffusion of both ions competes. After this temperature, up to melting and beyond that, magnesium ions clearly become more diffusive indicating that the size of the ions determines the diffusion. The average anion and cation transference numbers are estimated as $t_+ \cong 0.54$ and $t_- \cong 0.46$ exhibiting almost balanced contribution to conductivity.

The Arrhenius equation is widely used to model the ionic migration in the condensed matter which is given as $D_i = Aexp(-\Delta H/k_B T)$, where A and ΔH are the preexponential term and the activation enthalpy, respectively. The Arrhenius plot is shown in Figure 6 b. Two linear regimes at the solid and liquid phases are evident at the regions of 800–1750 K and 1800–2500 K, respectively. The activation energies are estimated from the slope of the linear regime as $E_{Mg} = 0.94$eV, $E_N = 0.82$eV at the solid phase and $E_{Mg} = 0.60$eV, $E_N = 0.62$eV at the liquid phase.

The linear thermal expansion coefficient (LTEC) α_T was calculated using the definitions $\alpha_T = \frac{1}{l_0}\left(\frac{dl}{dT}\right)$ and is presented in Figure 7. Figure 7(a) shows the detailed comparison of LTEC at the solid phase with two available experimental data, which are the ones recently reported for a single crystal in the 350–775 K range [36] and previously for $Mg_3\ N_2$ powder at low temperatures between 10 and 300 K [37]. Within the limitations of a classical rigid ion model potential, the LTEC reasonably agreed with experimental data and extended further for a wide range of temperatures. In addition, a marked sharp peak in the thermal expansion at 1800 K signifies the melting of the system.

The melting transition of magnesium nitride is also displayed as a peak at the same temperature in the heat capacity $C_P = \left(\frac{\partial E}{\partial T}\right)_P$ and the rate of entropy change $\left(\frac{\partial S}{\partial T}\right)_P$ (Figure 8). At low temperatures, C_P obeys the Dulong-Petit law with the classical value of ≈ 25 kJ/molK; then it increases slowly as a result of progressive excitations of the harmonic vibrations with increasing temperature while the rate of entropy change nonlinearly decreases. As the temperature approaches 1800 K, the anharmonicity of the vibrations is reflected as a weak but further increase signaling the onset of melting transition.

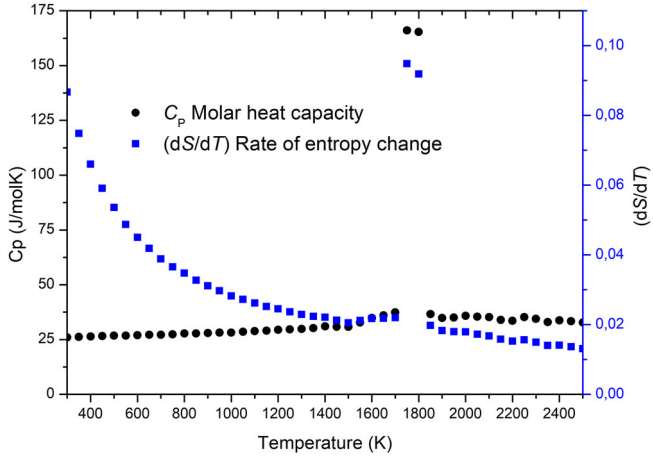


Figure 8. (Colour online) The heat capacity C_P and the rate of entropy change $\left(\frac{\partial S}{\partial T}\right)_P$.

4. Conclusions

Magnesium nitride (Mg_3N_2) is an attention drawing material with important physicochemical properties. Besides its applications as an additive to fabricate alloys, a catalyst to synthesise metal or non-metal nitrides and an optoelectronic light-emitting semiconducting material. It is also a potential candidate as a hydrogen storage material and electrolyte in the liquid metal battery. Therefore, it is crucial to assess thermophysical and ion transport characteristics of Mg_3N_2 at the solid and liquid phases. We have developed an interatomic pairwise potential based on a partially rigid ion model which is validated by the mechanical properties at 0 K and the NVE ensemble simulation at 300 K. Temperature evolution of the static structure, ionic transport and thermal properties are investigated by means of molecular dynamics simulation in the NPT ensemble between 300 K and 2500 K. Simulated X-ray powder diffraction peaks of Mg_3N_2 with corresponding Bragg angles and (hkl) planes match correctly with the XRD patterns of the combustion synthesised Mg_3N_2 powders.

All physical properties of Mg_3N_2 calculated using our model potential reflect the characteristic features of ionic solids and liquids, and exhibit distinct variation at about 1800 K signifying the melting. This is observed as a first-order structural transition from fourfold coordination with well-defined crystalline peaks to threefold coordination with little structure beyond less pronounced broad first peak in $g_{ij}(r)$ at liquid. The change of MSD from the zero asymptotic slope to linear growth with a sudden increase in self diffusion coefficients, and a sharp peak in both linear thermal expansion and specific heat capacity are the kinetic and thermodynamic evidence of the melting transitions, respectively. The potential model and physical properties presented in this paper fill the gap of theoretical study in literature and could be beneficial for future theoretical and experimental studies on magnesium nitride; for instance, to study the surface and subsurface adsorption of hydrogen, the diffusive transport of atoms at the interface of thin film materials and the liquid metal electrode–electrolyte interface for the optoelectronic and energy store applications – using the molecular dynamics simulation in conjunction with an already justified model potential – will be advantageous.

Acknowledgements

The authors would like to acknowledge that this paper is submitted in partial fulfilment of the requirements for PhD degree at Yildiz Technical University.

Disclosure statement

No potential conflict of interest was reported by the author(s).

References

[1] Lorenz H, Kuhne U, Hohlfeld C, et al. Influence of MgO on the growth of cubic boron nitride using the catalyst Mg_3N_2. J Mater Sci Lett. 1988;7:23–24.
[2] Parkin IP, Nartowski AM. Solid state metathesis routes to group IIIa nitrides: comparison of Li_3N, NaN_3, Ca_3N_2 and Mg_3N_2 as nitriding agents. Polyhedron. 1998;17:2617–2622.
[3] Nakano S, Ikawa H, Fukunaga O. High pressure reactions and formation mechanism of cubic BN in the system BN-Mg_3N_2. Diam Relat Mater. 1993;2:1168–1174.
[4] Bruls RJ, Hintzen HT, Metselaar R. Preparation and characterisation of $MgSiN_2$ powders. J Mater Sci. 1999;34:4519–4531.
[5] Lorenz H, Peun T, Orgzall I. Kinetic and thermodynamic investigation of c-BN formation in the system BN-Mg_3N_2. Appl Phys A-Mater. 1997;65:487–495.
[6] Kojima Y, Kawai Y, Ohba N. Hydrogen storage of metal nitrides by a mechanochemical reaction. J Power Sources. 2006;159:81–87.
[7] Nakamori KG, Miwa K, et al. Reversible hydrogen-storage functions for mixtures of Li_3N and Mg_3N_2. Appl Phys A-Mater. 2005;80(1):1–3.
[8] Chen P, Xiong Z, Luo J, et al. Interaction of hydrogen with metal nitrides and imides. Nature. 2002;420:302–304.
[9] Fang C M, de Groot R A, Bruls R J, et al. Ab initio band structure calculations of Mg_3N_2 and $MgSiN_2$. J Condens Matter Phys. 1999;11 (25):4833–4842.
[10] Schneider S B, Frankovsky R, Schnick W. Synthesis of alkaline earth diazenides MAEN2 (MAE = Ca, Sr, Ba) by controlled thermal decomposition of azides under high pressure. Inorg Chem. 2012;51:2366–2373.
[11] Bradwell DJ, Kim H, Sirk AHC, et al. Magnesium-antimony liquid metal battery for stationary energy storage. J Am Chem Soc. 2012;134(4):1895–1897.
[12] Ullah M, Murtaza G, Ramay SM, et al. Structural, electronic, optical and thermoelectric properties of Mg_3X_2 (X = N, P, As, Sb, Bi) compounds. Mater Res Bull. 2017;91:22–30.
[13] Dadsetani M, Beiranvand R. First principles study of the optical properties of alkaline-earth metal nitrides. Comput Mater Sci. 2010;49:400–406.
[14] Kayadibi F, Günay SD, Taşseven Ç. Studying static, dynamic and transport properties of Mg_3Bi_2. Acta Phys Pol A. 2015;128 (3):440–446.
[15] Akdere Ü, Günay SD, Taşseven Ç. Ordering and diffusion in liquid magnesium antimonide (Mg_3Sb_2) from hypernetted-chain theory and molecular dynamics simulation. Ionics. 2019;25:2711–2717.
[16] Günay SD. Thermophysical properties of magnesium arsenide with atomistic simulation methods. J Phys Chem Solids. 2021;148:109614.
[17] Reckeweg O, DiSalvo FJ. About binary and ternary alkaline earth metal nitrides. Z Anorg Allg Chem. 2001;627:371–377.
[18] Fumi FG, Tosi MP. Ionic sizes and born repulsive parameters in the NaCl-type alkali halides—I: the Huggins-Mayer and Pauling forms. J Phys Chem Solids. 1964;25(1):31–43.
[19] Gale JD, Rohl AL. The general utility lattice program (GULP). Mol Simul. 2003;29(5):91–341.
[20] Niu CW, Yang K. Electronic and magnetic properties of C-doped Mg_3N_2: a density functional theory study. Solid State Commun. 2010;150:2223–2226.
[21] Ullah M, Murtaza G, Ramay SM, et al. Structural, electronic, optical and thermoelectric properties of Mg_3X_2 (X:N, P, As, Sb. Bi) compounds. Mater Res Bull. 2017;91:22–30.
[22] Ji D, Chong X, Feng J. Electronic, mechanical and hydrogen storage properties of novel Mg_3N_2. J Alloys Compd. 2019;800:8–15.
[23] Partin DE, Williams DJ, O'Keeffe M. The crystal structures of Mg_3N_2 and Zn_3N_2. J Solid State Chem. 1997;132:56–59.
[24] Trivedi M K, Tallapragada R M, Branton A, et al. Evaluation of thermal and physical properties of magnesium nitride powder: impact of biofield energy treatment. Ind Eng Manag OMICS Int. 2015;4 (5):hal-01462835.
[25] Li J, Fan C, Dong X, et al. Theoretical investigation of the high – pressure structure, phase transition, and mechanical and electronic properties of Mg_3N_2. J Phys Chem C. 2014;118(19):10238–10247.
[26] Voigt W. Lehrbuch der Kristallphysik. Leipzig: Teubner; 1928.
[27] Reuss A. Berechnung der Fließgrenze von Mischkristallen auf Grund der Plastizitätsbedingung für Einkristalle. Z Angew Math Mech. 1929;9:49–58.
[28] Hill R. The elastic behaviour of a crystalline aggregate. Proc Phys Soc. 1952;A65:349–354.

[29] Hong SY, Fu C L. Phase stability and elastic moduli of Cr_2Nb by first-principles calculations. Intermetallics. 1999;7:5–9.
[30] Pugh SF. XCII. Relations between the elastic moduli and the plastic properties of polycrystalline pure metals. Philos Mag. 1954;45:823–843.
[31] Ingel RP, Lewis D. Elastic anisotropy in zirconia single crystals. J Am Ceram Soc. 1988;71(4):265–227.
[32] Refson K. A portable molecular dynamics simulation program for serial and parallel computers. Comput Phys Commun. 2000;126 (3):310–329.
[33] Ropp RC. Encyclopedia of the alkaline earth compounds. Oxford: Elsevier; 2013.
[34] Momma K, Izumi K. VESTA 3 for three-dimensional visualization of crystal, volumetric and morphology data. J Appl Crystallogr. 2011;44:1272–1276.
[35] Mei L, Li JT. Combustion synthesis of ultrafine magnesium nitride powder by Ar dilution. Scr Mater. 2009;60:141–143.
[36] John P, Rotella H, Deparis C, et al. Crystalline magnesium nitride (Mg_3N_2): from epitaxial growth to fundamental physical properties. Phys Rev Mater. 2020;4:054601.
[37] Paszkowicz W, Knapp M, Domagala J Z, et al. Low-temperature thermal expansion of Mg_3N_2. J Alloys Compd. 2001;328:272–275.